

# Evaluation of the Spatio-Temporal features and GAN for Micro-expression Recognition System

Sze-Teng Liong<sup>a</sup>, Y.S. Gan<sup>b</sup>, Danna Zheng<sup>c</sup>, Shu-Meng Li<sup>c</sup>, Hao-Xuan Xu<sup>c</sup>, Han-Zhe Zhang<sup>c</sup>, Ran-Ke Lyu<sup>c</sup>, Kun-Hong Liu<sup>d,\*</sup>

<sup>a</sup>Department of Electronic Engineering, Feng Chia University, Taichung, Taiwan

<sup>b</sup>Research Center for Healthcare Industry Innovation, NTUNHS, Taipei, Taiwan

<sup>c</sup>School of Electrical and Computing Engineering, Xiamen University Malaysia, Jalan Sunsuria, Sepang, Selangor, Malaysia

<sup>d</sup>School of Software, Xiamen University, Xiamen, China

## Abstract

Owing to the development and advancement of artificial intelligence, numerous works were established in the human facial expression recognition system. Meanwhile, the detection and classification of micro-expressions are attracting attentions from various research communities in the recent few years. In this paper, we first review the processes of a conventional optical-flow-based recognition system, which comprised of facial landmarks annotations, optical flow guided images computation, features extraction and emotion class categorization. Secondly, a few approaches have been proposed to improve the feature extraction part, such as exploiting GAN to generate more image samples. Particularly, several variations of optical flow are computed in order to generate optimal images to lead to high recognition accuracies. Next, GAN, a combination of Generator and Discriminator, is utilized to generate new “fake” images to increase the sample size. Thirdly, a modified state-of-the-art convolutional neural networks is proposed. To verify the effectiveness of the the proposed method, the results are evaluated on spontaneous micro-expression databases, namely SMIC, CASME II and SAMM. Both the F1-score and accuracy performance metrics are reported in this paper.

*Keywords:* apex, CNN, GAN, micro-expression, optical flow, recognition

## 1. Introduction

Micro-expression (ME) is a kind of natural human expression that normally occurs when a person tries to conceal his or her genuine emotion. Different from other genuine expressions, MEs are the tiny movements of facial muscles and usually last for half a second [1]. Due to its uncontrollable and involuntary characteristics, MEs always show the real feelings of a person. Thus, recognizing ME helps the researchers especially in the psychology aspect to discover hidden insights. Besides, MEs recognition are applied to several fields, such as the police interrogation [2], psychological clinical diagnosis [3], social interaction [4], judicial system [5], political elections [6] and national security [7]. However, due to the subtlety and rapid attributes, it poses a great challenge for normal people to notice the occurrence of ME from their naked eyes in the real-time conversations. Similar to the normal facial expression, a.k.a., macro-expression, it can be classified into six basic emotions: happy, sad, surprise, fear, anger and disgust. In brief, ME is first discovered in 1969, when Ekman [8] analyzed an interview video of a psychotherapist

and a patient who attempted to commit suicide. When Ekman watched the video frame by frame, he found out that the patient tried hide her sad feeling by covering up with smile during the interview process. Later, Ekman and Friesen [9] created a model called Facial Action Coding System (FACS) to identify each action units (AUs). Action unit describes the facial muscle motions in certain direction.

Classically, an automatic ME recognition system is divided into two steps: ME spotting and ME recognition. The former is to identify the ME interval or some specific important frames; while the latter is to perform the emotion class classification. Currently, there are many methods proposed in literatures to perform the ME spotting and recognition tasks. Thus far, the highest recognition accuracy achieved is 78.14%, which is conducted by Li et al. [10] using the HIGO method and SVM classifier. Hence, there is still room for improvement to build a better system.

## 2. Related Work

This section reviews the micro-expression databases, discusses the techniques used in ME spotting and recognition, and analyzes the problems faced in the previous works.

\*Corresponding author

Email addresses: stliong@fcu.edu.tw (Sze-Teng Liong), ysgn88@gmail.com (Y.S. Gan), lkhqz@xmu.edu.cn (Kun-Hong Liu)

## 2.1. Database

To date, there are six popular ME databases established for the researchers especially from computer vision field for algorithm development and analysis. The databases included USF-HD [11], SMIC [12, 13], CASME [14], CASME II [15], CAS(ME)<sup>2</sup> [16] and SAMM [17]. The brief information of these six databases are shown in Table 1. Among the six databases, CASME II has the most abundant samples that contains 247 videos and it is commonly served as the baseline database for algorithm evaluation. It is observed that the database are having small data size. This is because some emotions are more likely to trigger, resulting in uneven distribution of samples. On the other hand, the ethnic and geographical distribution of the participants in each database are different, hindering the development of feature extractors methods and it is also difficult for data generalization.

## 2.2. Micro-Expression System

An ME micro-expression system comprised of three main basic stages, which are pre-processing, feature extraction and classification namely. The pre-processing techniques include the face detection and registration, face masking and regions of interest acquisition, important frames selection. Most of the research works focus on improving the feature extractors, compared to the pre-processing and classification stages. Feature extraction is to represent an image with minimum feature dimension whilst retaining meaningful ME details. The feature extractors can be categorized into handcrafted and deep learning methods. The following subsections elaborate the state-of-the-arts of these three stages.

### 2.2.1. Pre-processing

*Face detection and registration.* To detect the position of the face, the landmarks of the face are first located. The example of the face with landmark coordinates annotated is shown in Figure 1 [18]. It can be seen that there is a total of 68 labeled locations on the face. Prototypically, there are three techniques commonly used in locating the facial landmark points, namely: Active Shape Model (ASM) [19], Active Appearance Model (AAM) [20] and Discriminative Response Map Fitting (DRMF) [21].

ASM is an algorithm based on the Point Distribution Model (PDM). Basically, it first selects the landmarks from a training set manually. Then, a feature-based method, Procrustes[22], is employed for face alignment and registration. It constructs the local features for each landmark to iteratively search new landmarks and obtains the shape model. An advantage of the model is that it has significant constraints on the contour shape. However, its iteratively search strategy limits the computational efficiency. AAM model is an improved version of ASM by adding the texture features from the entire face area. On the other hand, DRMF is based on the Cascade Pose Regression [23] that uses the Support Vector Regression (SVR) [24] to model

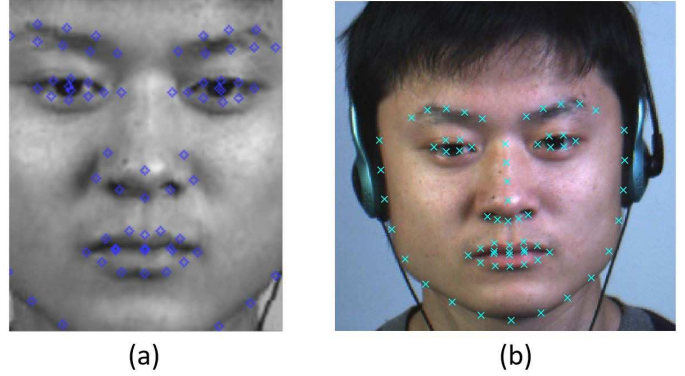


Figure 1: Example of locating the landmark coordinates using: (a) Face++, and (b) DRMF

a regression function. It adopts the shape-dependent Histogram of Gradient (HOG) [25] features as the input to cascade the predicted face shape. There are a few online tools such as Face++ [26] and Openface [27], which are executed in real-time performance without installing any specialist hardware.

In 2013, Sun et al. [28] applied convolutional neural network (CNN) for face landmark detection and proposed a cascaded CNN (with three levels). Since the CNN has superior abilities of feature extraction, it is more precise and robust in the landmark detection and resolve the local optimal issues. However, it fails to deal with the occlusion problems. On the other hand, Huang et al. [29] introduced an algorithm from coarse to fine to divide the face landmarks into internal landmarks and contour landmarks, using the Face++, and it leads to high-precision positioning. In 2016, Zhang et al. [30] presented a multi-task Cascaded Convolutional Networks (MTCNN) to simultaneously conduct face detection and face landmarks detection. Concisely, it consists of three cascaded multitasking CNN: Proposal Network (P-Net), Refine Network (R-Net), and Output Network (O-Net). A year later, Kowalski et al. [31] proposed a new cascaded deep neural network, Deep Alignment Network (DAN). By adding a landmarks heat map as a supplement, DAN extracts the features from the whole picture to obtain more accurate landmark positioning. However, there is a significant disadvantage in these three methods, which is a high computational complexity due to the complicatedness of the mathematical derived operations.

For the face registration, there exists two approaches: area-based method and feature-based method. The former method is based on the correspondence of the entire image, such as 2D-DFT[32], while the latter is based on the correspondence of regions, points, and line features (i.e., affine transform, Local Weighted Mean[33] and Procrustes analysis).

*Face Masking and Region Partitioning.* Face masking is to reduce the effects of irrelevant factors that do not correspond to the desired facial movements. To eliminate the

Table 1: Available Micro-expression Databases

Database	Year	# Participant	# Video	Frame Rate	Resolution	# Emotion
USF-HD	-	-	100	30	170×1280	6
SMIC	2013	16	164	100	640 × 480	3
CASME	2013	35	195	60	640 × 480	7
CASME II	2014	35	247	200	640 × 480	5
CAS(ME) <sup>2</sup>	2018	22	57	30	640 × 480	4
SAMM	2018	32	159	200	2040 × 1088	7

noise generated from the eye blinking motions, Shreve et al. [11] and Liong et al. [34] proposed to mask the eye regions for each image. In addition, [11] covers other regions such as nose and mouth with a T-shaped mask. Davison et al. [32] identified 26 FACS-based facial regions heuristically to facilitate the facial feature localization. Moilanen et al. [35], Davison et al. [36, 17], Wang et al. [37], Liong et al. [38] and Li et al. [10] divided the entire face into several equal parts. On the other hand, Polikovskiy et al. [39, 40], Liong et al. [41, 34, 42, 43], Davison et al., [32] and Li et al. [44] selected certain region-of-interests (RoIs) from the face. Generally, the method with RoIs partitioning yields to promising performance as it is better to represent the local feature efficiently.

*Frames selection and Magnification.* Since the MEs are very subtle, most of the sample videos are elicited using a high frame rate camera. Repetitive frames with very little changes in movements might result in data redundancy. In other words, not all the frames are important. A frame selection step dynamically choose the significant frame that contain meaningful expression details. For instance, Temporal interpolation method (TIM) [46, 12, 47, 10] is often used in the previous experiments to standardize the frame length for all videos. On another note, Le Ngo et al. [48] show that the recognition accuracy is improved by applying Sparsity-Promoting Dynamic Mode Decomposition (DMDSP). They demonstrate that DMDSP is effective when interpolating small number of frames, but larger number of frames degrades the recognition performance because of over interpolation. To enlarge the subtle motion changes of MEs, motions magnification operation can be applied, such as the Eulerian Video Magnification (EVM) [49]. An improved version of EVM, namely, Global Lagrangian Motion Magnification (GLMM), is recently utilized by Le Ngo et al. [50], whereby they report that higher ME recognition accuracy results can be achieved.

### 2.2.2. Feature Extraction

*Handcrafted Approach.* Many pioneer ME research works [12, 13, 14, 15, 16, 17] applied Local Binary pattern (LBP) variants to evaluate the videos collected. LBP is a feature descriptor that effectively represents

a two-dimensional gray-scale image in a compact binarized vector. The LBP family includes LBP [51], Local Binary Pattern on Three Orthogonal Planes (LBP-TOP) [12, 52, 53], Local Binary Pattern with Six Intersection Points (LBP-SIP) [54], Local Binary Pattern with Mean Orthogonal Planes (LBP-MOP) [55], Discriminative Spatiotemporal Local Binary Pattern with Revised Integral Projection (DiSTLBP-RIP) [56] and Spatiotemporal Completed Local Quantization Patterns (STCLQP) [57]. LBP is insensitive to illumination change, computational simplicity, capable of handling a variety of spatial information, robust to rotation and translation. LBP-TOP extracts features from both the spatial and temporal perspectives, for instance, from the three planes (XY, XT, YT planes). To reduce some of the duplicated computation in LBP-TOP, LBP-SIP is introduced to consider six neighboring unique points for each centre pixel. Thus, it produces 2.4 times lesser feature length per video compared to LBP-TOP yet with higher recognition on SMIC and CASME II datasets. LBP-MOP computes three mean images for each video and it outperforms LBP-TOP on CASME II dataset. Notably, the average time for extracting the features in each video using LBP-MOP is 38 times faster than that of LBP-TOP. On the other hand, DiSTLBP-RIP is a combination of LBP with integral projection and a comparable accuracy is achieved with simpler computation. STCLQP is mathematically more complex than LBP-TOP, because it collects more information which are sign, magnitude and orientation components. Wang et al. [58] extracted LBP-TOP features with Tensor Independent Color Space (TICS) and discovered that the recognition performance in TICS is better than that in both RGB and gray-scale. Generally, LBP-based methods are widely used, but it does not reflect the motion changes from certain face muscles intuitively.

Aside from LBP family, there is an optical flow family which are commonly utilized in ME recognition system. Basically, optical flow describes the apparent motion of the facial muscle movements based on the brightness patterns. The example of the optical flow family consists of Optical Strain Feature (OSF) [38], Optical Strain Weight (OSW) [38], Fuzzy Histogram of Oriented Optical Flow

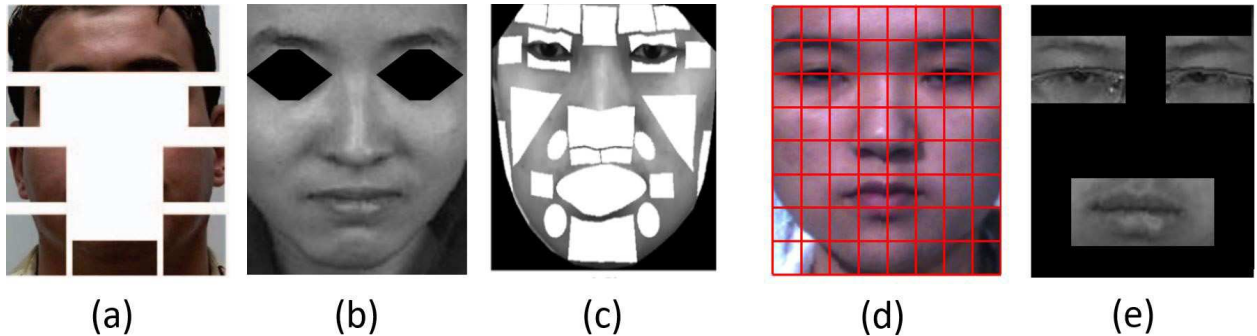


Figure 2: Example of the face masking and partitioning: (a) A T-shaped mask is applied to obtain the eight important regions [11]; (b) The eyes are masked to avoid eye blinking [34]; (c) The face is divided into 26 regions [32]; (d) The face is partitioned into several equal parts [38]; (e) Only the eyes and mouth regions are considered [45]

(FHOOF) [59], Fuzzy Histogram of Optical Flow Orientations (FHOFO) [59], Bi-weighted Oriented Optical Flow (Bi-WOOF) [42], Facial Dynamics Map (FDM) [60] and Main Directional Mean Optical flow (MDMO) [61]. Particularly, FHOOF, FHOFO, MDMO are insensitive to illumination changes and have better performance than LBP-TOP and HOOF. However, the weight assigned to FHOOF is highly dependent on motion magnitudes of various MEs, yet, FHOFO overcomes this drawback. In [42], Liong et al. proposed to use Bi-WOOF to extract the significant features and demonstrated that using onset and apex frames to represent the entire video sequence is feasible.

On the other hand, there is a gradient-based family which computes changes of the adjacent frames and produce the output in both the horizontal and vertical directions. The gradient-based features includes 3D-gradient [39], Histograms of Oriented Gradients (HOG) [62] and Histogram of Image Gradient Orientation (HIGO) [10]. HIGO is simpler and less susceptible to illumination changes compared to HOG. [10] shows that both the HOG and HIGO outperform LBP-TOP in CASME II dataset. Gradient-based features evolved from holistic-based to local-based. They have similar limitations with LBP-based family: the pixel-level attention.

*Deep Learning Approach.* Deep learning architecture has attracted much attention from the computer vision communities due to its viability in a broad range of applications. Concretely, for the ME recognition system, Peng et al. [63] suggest a Dual Temporal Scale Convolution Neural Network (DTSCNN) that comprised of two streams CNN to accommodate the input data with different frame rate. The results show that DTSCNN outperforms STCLQP, MDMO, and FDM by approximately 10% in accuracy performance metric. Kim et al. [64] proposed to combine CNN with long-term memory (LSTM) and remarkable results are obtained. It has been demonstrated that shallow CNN architectures are practically workable in the ME recognition system [65, 66, 67, 68]. Overall, although the transfer learning [69] and data augmentation [70] are performed, the limited number and imbalance emotion class distribution issues pose a great challenge to develop robust feature

extractors.

### 2.2.3. Classification

Classification stage is to categorize the emotion of a video according to the feature extracted. Support Vector Machine (SVM) [71] is the most popular classifier adopted in ME recognition system. Compared to other classifiers such as Random Forest (RF) [72], sparse representation classifier (SRC) [73] and Relaxed K-SVD [74], SVM appears to be more consistent across all the databases with distinct features extracted. Due to the emergence of deep learning, the Softmax classifier, normally served as the final fully connected layer, has been employed in the recent works [64, 75, 67, 66]. Its outstanding discriminative characteristics is beneficial, especially in dealing the high-level features.

## 3. Methodology

This section discusses the methods used for the whole process of micro-expression recognition. The flowchart of the proposed approach is illustrated in Figure 3. There are three primary objectives in this paper:

1. An analysis of both the sparse and dense optical flow methods and discover the effect towards the ME recognition system.
2. To increase the data sample size, several Generative Adversarial Network (GAN) approaches are exploited to generate “fake” optical flows images.
3. Implementation of a state-of-the-art CNN architecture and modification of the structure for feature enhancement and classification operations.

Details of each step are explained in the following subsections.

### 3.1. Apex frame spotting

Inspired by [42, 65], only two frames, viz., the onset and apex frame are selected to represent the whole video clip. The main advantages of utilizing two frames per video are computational simplicity, high efficiency and redundancy

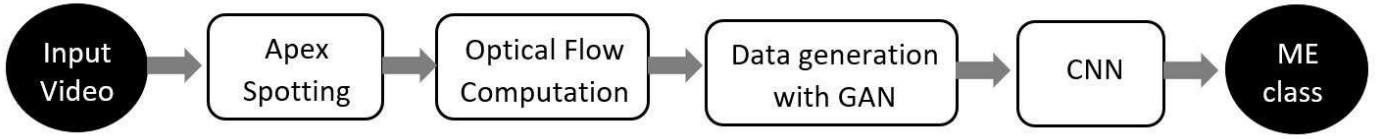


Figure 3: Flow diagram of the proposed methodology

elimination. Apex frame is the instant indicating of the most expressive emotional state in a video. Theoretically, the apex frame portrays the highest facial muscle movement changes compared to the onset frame. Onset frame is the moment denoting the beginning of an emotion. To spot the apex frame, we directly adopt the Divide & Conquer (D&C) method proposed by Liong et al. [42]. Concretely, the algorithm consists five steps: 1) Multiple local peaks of whole video clips are determined; 2) Frame sequence is divided into two halves equally (i.e., a 40 frames video sequence is split into two sub sequences containing frame 1-20 and 21-40); 3) Magnitude of the detected peaks are summed up for each of the sub sequence; 4) The sub sequence with the higher magnitude will be remained and the other sub sequence will be neglected; 5) Step 2 to 4 are repeated until the single final frame is identified.

### 3.2. Optical Flow Computation

Optical flow describes the dynamic changes of an object and represent the movements using a two-dimension vector field (i.e., horizontal and vertical optical flows). There are several optical flow methods in the literature, namely, Robust Local Optical Flow (RLOF) [76], Horn & Schunck [77], TVL1 [78], Farneback [79], LiteFlowNet [80], PWC-Net+ [81], FlowNet [82] and Lucas Kanade [83]. Among the optical flow methods, we exploit Farneback, Horn & Schunck, Lucas Kanade, TVL1 and RLOF to compute the flow fields of the onset and apex frames for all the video sequence. The horizontal and vertical optical flow are expressed as  $(p, q)$ . There are three other optical flow properties that can be derived from  $(p, q)$ : magnitude, orientation and optical strain. Succinctly, to obtain the magnitude and orientation, the horizontal and vertical flow components,  $\vec{\sigma} = (p, q)$ , are converted from Euclidean coordinates to polar coordinates:

$$\rho_{x,y} = \sqrt{p_{x,y}^2 + q_{x,y}^2}, \quad (1)$$

and

$$\theta_{x,y} = \tan^{-1} \frac{q_{x,y}}{p_{x,y}}, \quad (2)$$

where  $\rho_{x,y}$  and  $\theta_{x,y}$  are the magnitude and orientation respectively.

In terms of displacements, the optical strain ( $\varepsilon$ ) is expressed as:

$$\varepsilon = \frac{1}{2}[\nabla \mathbf{u} + (\nabla \mathbf{u})^T] \quad (3)$$

or can be formulated as:

$$\varepsilon = \begin{bmatrix} \varepsilon_{xx} = \frac{\partial u}{\partial x} & \varepsilon_{xy} = \frac{1}{2}(\frac{\partial u}{\partial y} + \frac{\partial v}{\partial x}) \\ \varepsilon_{yx} = \frac{1}{2}(\frac{\partial v}{\partial x} + \frac{\partial u}{\partial y}) & \varepsilon_{yy} = \frac{\partial v}{\partial y} \end{bmatrix} \quad (4)$$

where the diagonal strain components,  $(\varepsilon_{xx}, \varepsilon_{yy})$  are normal strain components and  $(\varepsilon_{xy}, \varepsilon_{yx})$  are shear strain components. Normal strain measures the changes in length along a specific direction, whereas shear strains measure the changes in two angular directions.

### 3.3. Data Generation with GAN

To evaluate the robustness of a feature extractor, [66] combines the video samples from three databases with different nature. Specifically, CASME II, SMIC and SAMM are combined into a composite database, therefore, it contains 442 videos and three emotion classes (i.e., positive, negative and surprise) from 68 participants. To further increase the size of input sample to the classifier, a neural network, namely, GAN is utilized to automatically generate new optical flow images. Particularly, two GAN network structures are experimented: (1) Auxiliary Classifier GAN (AC-GAN) [84], and; (2) Self-Attention GAN (SAGAN) [85].

The main idea of GAN is from a two-player game, where one acts as the generator model, the another one is served as the discriminator model. In brief, a random noise  $z$  is first input into the generator model and output an image  $A$ . Then, the real image  $B$  together with the image  $A$  is passed to the discriminator, it produces the probability contributions over its truth degree and over the real image. The aim of the generator is to generate an image as real as possible, and the discriminator attempts to distinguish the correctness of the real and fake generated images. After several repetitions of training processes, an discriminator outputs probability of 0.5 would be expected to indicate the balance of the model. The pseudocode of the GAN algorithm is listed in Algorithm 1. In each of the game, the discriminator produces either 1 or 0 by function  $g$ :

$$g(x) = \begin{cases} 1, & x = \text{Real Image} \\ 0, & x = \text{Fake Image} \end{cases} \quad (5)$$

Note that, throughout the GAN learning process, back propagation is employed to reduce the training losses by optimizing the weights of the neurons.

---

**Algorithm 1** Generative Adversarial Networks

---

```
1:  $k \leftarrow$  step
2:  $K \leftarrow$  number of training iterations
3: repeat
4:   repeat
5:     Sample  $m$  noise samples  $\{z^{(1)}, \dots, z^{(m)}\}$  from noise prior  $\delta_g(z)$ 
6:     Sample  $m$  examples  $\{x^{(1)}, \dots, x^{(m)}\}$  from noise prior  $\delta_{data}(x)$ 
7:     Update the discriminator via stochastic gradient:
8:      $\nabla_{\theta_d} \frac{1}{m} \sum_{i=1}^m [\log D(x^{(i)}) + \log (1 - D(G(z^{(i)})))]$ 
9:
10:   until  $k = K$ 
11:   repeat
12:     Sample  $m$  noise samples  $\{z^{(1)}, \dots, z^{(m)}\}$  from noise prior  $\delta_g(z)$ 
13:     Update the generator via stochastic gradient:
14:      $\nabla_{\theta_g} \frac{1}{m} \sum_{i=1}^m [\log (1 - D(G(z^{(i)})))]$ 
15:
16:   until  $k = K$ 
17: until the stopping criterion is met
```

---

The brief introductions of AC-GAN and SAGAN are explained as follows:

### 1. Auxiliary Classifier GAN

Odena et al. [84] suggest an objective function where the log-likelihood of the correct source, LS, and the log-likelihood of the correct class, LC are defined as:

$$L_S = E[\log P(S = \text{real} | X_{\text{real}})] + E[\log P(S = \text{fake} | X_{\text{fake}})], \quad (6)$$

and

$$L_C = E[\log P(C = c | X_{\text{real}})] + E[\log P(C = c | X_{\text{fake}})] \quad (7)$$

The discriminator and generator are optimized by maximizing the  $L_S + L_C$  and  $L_C - L_S$ , respectively. The example of the AC-GAN structure is illustrated in Figure 4.

### 2. Self-Attention GAN

SAGAN is a model that improved by the Natural-Language Processing (NLP) where uses attention to focus on certain important areas on the image. For traditional convolution GAN, the convolution operation is suitable for processing neighborhood information because of the restriction of receptive field limit. However, the feature correlation of pixels that are far apart requires several convolutional layers. The model is not able to capture the global information if the convolution kernel is not large enough. In contrast, if the kernel is considerably large, it requires more computation time and leads to low efficiency. SAGAN utilizes

the image information from all feature locations to generate image detail, and at the meantime, ensures that the discriminator is capable to identify the consistency between two features that are far from each other. In addition, a normalization operation is carried out to enhance the stability and efficiency during the model training process.

### 3.4. Convolutional neural network for Feature Classification

A typical convolutional neural network (CNN) consists of several pairs of convolutional layer and pooling layer followed by some fully connected layers. The convolutional and pooling layers are used for feature enhancement or feature extraction. Concisely, each convolutional layer is made up of several kernels or filters (i.e., usually 6, 16, 32 or 64 kernels, depends on the context of the input image). The kernels are the matrices, a.k.a., the weights, which will be multiplied to the input image. As a result, the original input image becomes “thicker” or “deeper”. In order to reduce the information redundancy, the common practice is to place a pooling layer after each convolutional layer. A pooling layer consists of certain kernel number, but here the kernels’ function is to scan the inputs and identify the most representative value in a certain pixels region. For instance, after the applying a  $2 \times 2$  pooling layer kernel on a  $2 \times 2$  image produced by the convolutional layer, the image will be reduced to a single number. There exists a variety of pooling methods, such as max pooling, min pooling and stochastic pooling. An example of a simple CNN architecture that comprised of two pairs of convolutional and pooling layers is illustrated in Figure 5.

Conventionally, after the input image passes through a few pairs of convolutional and pooling layers, one or more fully connected layer are then placed. A fully connected

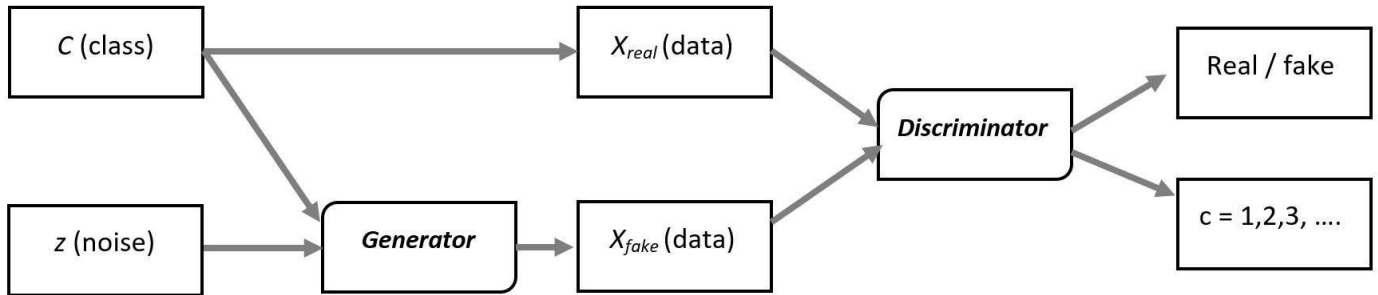


Figure 4: Auxiliary classifier GAN (AC-GAN) architectures, where  $x$  is the real image,  $c$  the class label and  $z$  the noise vector

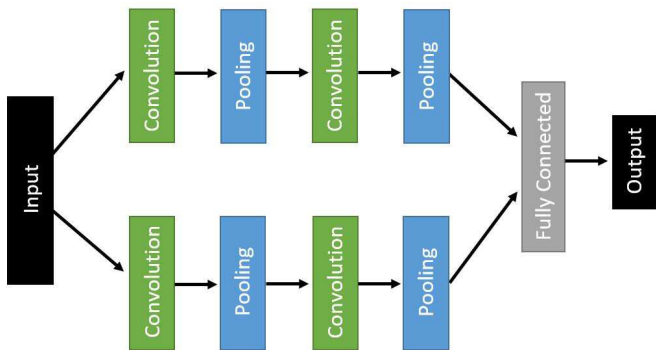


Figure 5: Example of a CNN architecture that comprised of two pairs of convolutional and pooling layers

layer accepts matrices as inputs, it connects every input matrix to all the existing output channels. This fully connected layer also served as the classifier to produce corresponding emotion classes as the output. In order to avoid the phenomena of overfitting or underfitting in the CNN model training process, the loss function will be observed according to the difference between the predicted emotion class attained by the network and the true emotion class. The gradient of the loss is calculated, which will be back propagated to every kernel. At the same time, the weights (i.e., in convolutional layers and fully connected layers) will be updated. The training process is terminated when training loss gradually decreases across the training iteration (i.e., epoch).

We tend to enhance the OFF-ApexNet [65] architecture to improve the recognition results. The OFF-ApexNet accepts the horizontal and vertical optical flow images, then passes them to two streams of the convolutional and max pooling layers. The outputs of both parallel layer sets are concatenated to serve as the input to the three fully connected layers. To compare the recognition performance of the original OFF-ApexNet architecture to the modified version, a re-implementation of original OFF-ApexNet is conducted and results are reported in the experiment section later. In particular, the modifications made on the OFF-ApexNet are listed as follows:

1. A parallel stream is added which allows to take in another type of optical flow information (i.e., magnitude,

orientation, optical strain, etc.). Thus, instead of only extracting the features from two directions of the optical flows ( $p, q$ ), CNN can learn more ME details and provide more clues for the ME characteristics.

2. Rather than concatenating the output features at the beginning of the fully connected layer, a multiplication operation is used to reduce the dimension of the features whilst maintaining the features quality.
3. A visualization of features in different layers is implemented and the principle component analysis is conducted for the classification output. With these extra functions added to the model, the whole training process would seem to be more convincing due to the network transparency. Consequently, the mistakes made and the ambiguous behaviors during the training process are easily inspected and spotted.

The modified OFF-ApexNet architecture is illustrated in Figure 6.

#### 4. Experiment Setup

Multiple results analysis on different perspectives are conducted in this paper. First, we investigate the effect of different types of optical flow method by fixing all the other variables (i.e., the feature extractors and classifier) to constant. Secondly, the output images generated by AC-GAN and SAGAN are tested to verify its effectiveness in capturing the ME details. Thirdly, to examine the recognition performance by varying the input to the modified OFF-ApexNet. All the analysis are evaluated on a SVM with Leave-One-Subject-Out Cross Validation (LOSOCV) protocol. Concisely, the video sequence of one subject is treated as the testing data and the rest are categorized as the training data. This process is repeated for  $i$  times, where  $i$  is the number of subjects in the database. Then, the recognition results for all subjects are averaged to become the final resultant recognition accuracy. The average accuracy is defined as:

$$\text{Accuracy} := \frac{\text{TP} + \text{TN}}{\text{TP} + \text{TN} + \text{FN} + \text{FP}}, \quad (8)$$

where TP, TN, FN and FP are the true positive, true negative, false negative and false positive, respectively. Due

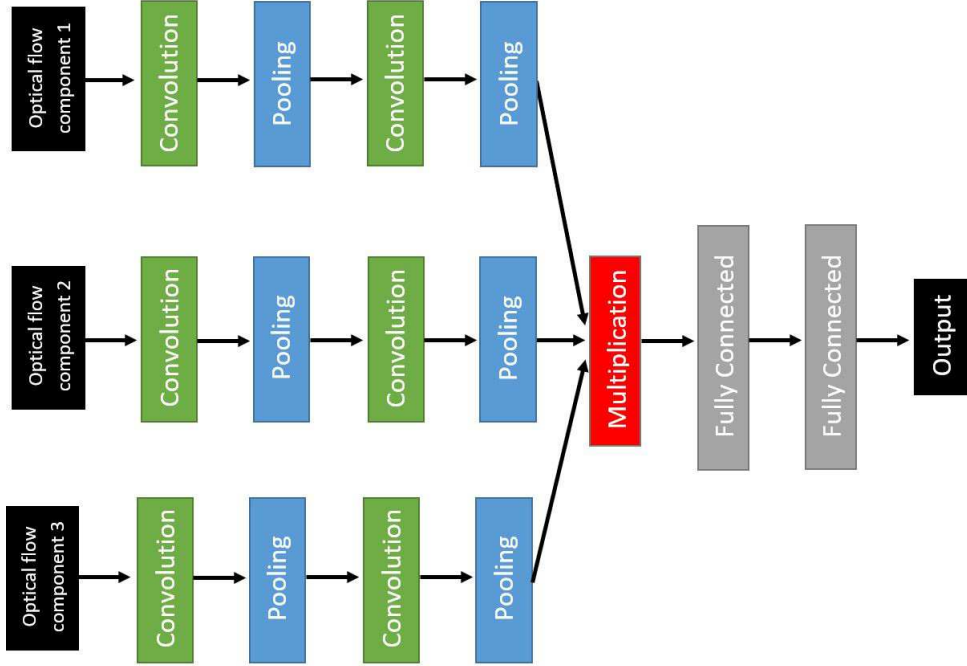


Figure 6: The modified OFF-ApexNet architecture

to the imbalance class distribution, F1-score performance metric is computed:

$$\text{F-measure} := 2 \times \frac{\text{Precision} \times \text{Recall}}{\text{Precision} + \text{Recall}}, \quad (9)$$

for

$$\text{Recall} := \frac{\text{TP}}{\text{TP} + \text{FN}}, \quad (10)$$

and

$$\text{Precision} := \frac{\text{TP}}{\text{TP} + \text{FP}}, \quad (11)$$

where TP, FN and FP are the true positive, false negative and false positive, respectively.

The details of the experimental setup is elaborated as follows:

#### 4.1. Optical Flow computation

In our experiments, five types of optical flow methods are computed, namely Farneback, Lucas Kanade and Horn & Schunck, TVL1 and RLOF. The example of horizontal and vertical optical flow images generated from the onset and apex frames are shown in Figure 7. It can be seen that Horn & Schunck and Lucas Kanade have similar visualization, whereas it is obvious that there is a lip corner movement in TVL1 images. On the other hand, the example of the nine optical flow variants generated from the same video sequence is illustrated in Figure 8. Specifically, the participants in this video shows a happiness emotion and the action unit triggered is 12 (i.e., the lip corner puller). It can be observed that most of the images in Figure 8 shows obvious movement, or has brighter color at the lip corner region.

We opt to conduct the experiments of this distinct type of optical flow approaches on SMIC database. Note that, the optical flow are derived from the onset and apex frames using the steps mentioned in Section 3.1. All the 164 video clips from SMIC are considered and three emotion classes involved are surprise, positive and negative. Then, the derived  $(\rho, \theta, \varepsilon)$  components are served as the input for the Bi-WOOF feature extractor [42] to for feature representation and SVM classifier for ME prediction.

#### 4.2. GAN for Data Augmentation

AC-GAN and SAGAN are chosen to artificially construct more data sample. Specifically, only the horizontal and vertical optical flow images are taken into consideration, and they are being trained by the GANs model separately. The emotion classes and random noise are first fed into the generator. Next, the same emotion class and the fake images produced by the generator are passed to discriminator to train the GAN model. Through this, the two individual network structures obtained (i.e., horizontal and vertical optical flow) can be used to create any number of fake images. The example of the AC-GAN and SAGAN generated images are shown in Figure 13 and Figure 14, with the annotated emotion class and optical flow components. The goal is to produce the training set to cope with the emotion class imbalance issue. The experiments of adopting GAN are conducted on SMIC database. Then, the Bi-WOOF feature extractor and SVM classifier are adopted to produce the final recognition results.

#### 4.3. Input to the Modified OFF-ApexNet

The original OFF-ApexNet was initially evaluated on the composite database which comprised of CASME II,



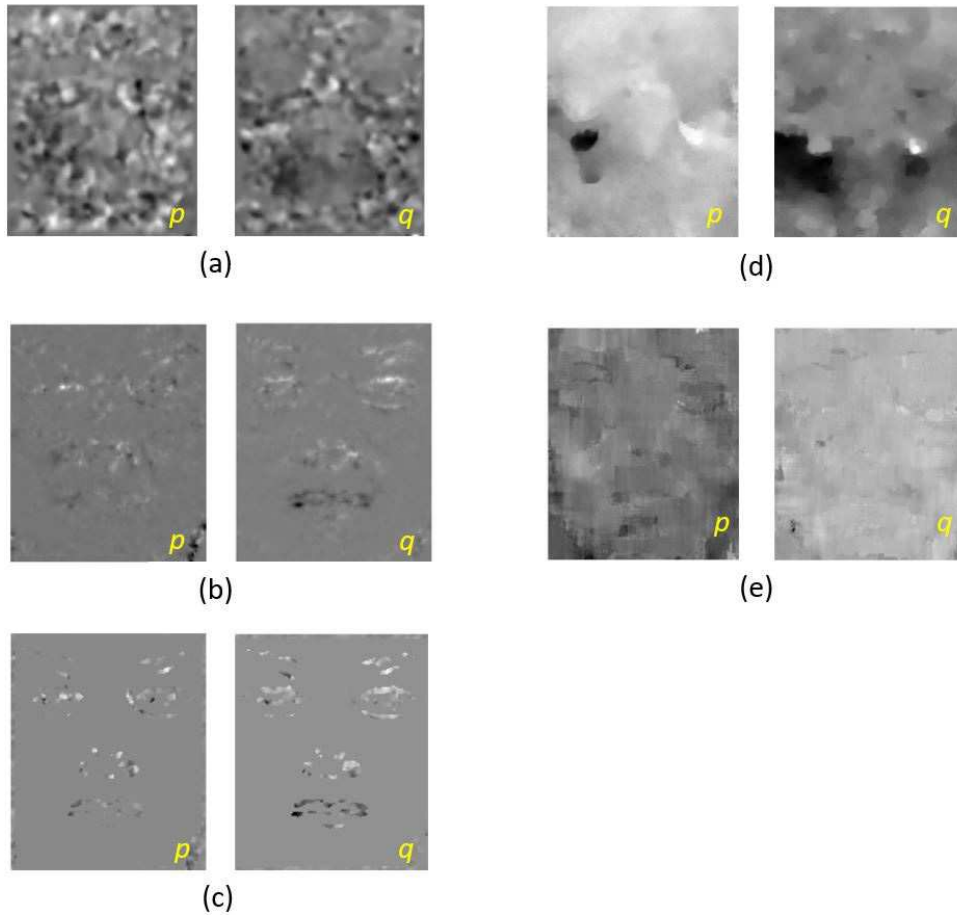


Figure 7: The horizontal and vertical optical flow derived images ( $p$  and  $q$ ) of a participant with subtle lip corner puller motion: (a) Farneback; (b) Horn & Schunck; (c) Lucas Kanade; (d) TVL1, and; (e) RLOF

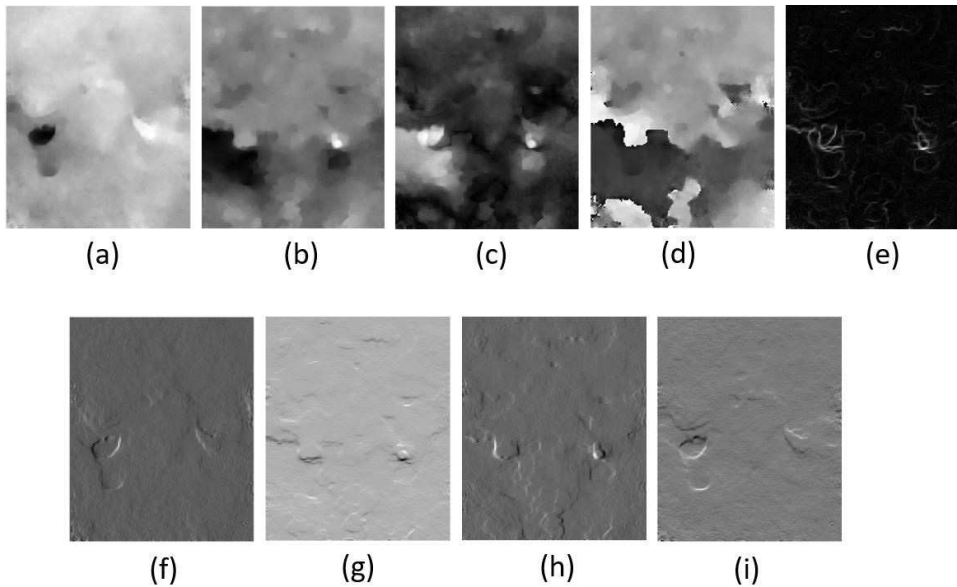


Figure 8: The optical flow derived images of a participant with happiness emotion: (a)  $p$ ; (b)  $q$ ; (c)  $\rho$ ; (d)  $\theta$ ; (e)  $\varepsilon$ ; (f)  $\varepsilon_{xx}$ ; (g)  $\varepsilon_{yy}$ ; (h)  $\varepsilon_{yx}$ ; (i)  $\varepsilon_{xy}$

SMIC and SAMM databases. There are a total 68 subjects with a total of 442 video clips. The nine optical flow com-

ponents (i.e., shown in Figure 8) are first extracted. Then they are normalized and reshaped into a  $n \times 28 \times 28 \times 1$



Figure 9:  $RLOF_u$



Figure 10:  $RLOF_v$

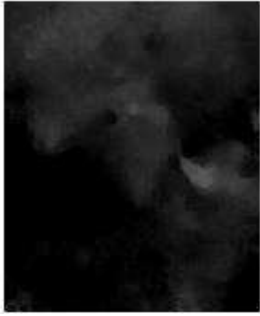


Figure 11:  $TVL1_u$

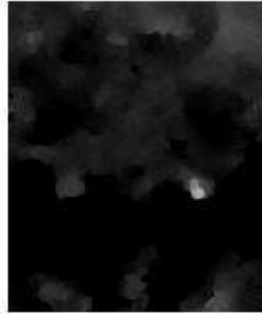
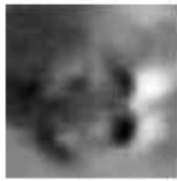


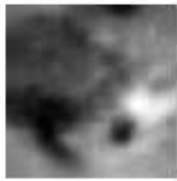
Figure 12:  $TVL1_v$



u\_class0



v\_class0



u\_class1



v\_class1

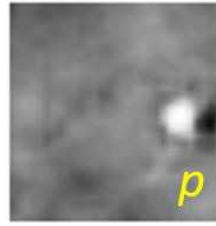


u\_class2



v\_class2

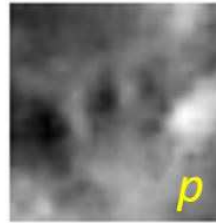
Figure 13: Fake images of AC-GAN



Surprise



Positive



Negative

Figure 14: Fake images of SAGAN

Table 2: Original OFF-ApexNet configuration [65]

Layer	Filter size	Kernel size	Stride	Padding	Output size
Conv 1	$5 \times 5 \times 1$	6	[1,1,1,1]	Same	$28 \times 28 \times 6$
Pool 1	$2 \times 2$	-	[1,2,2,1]	Same	$14 \times 14 \times 6$
Conv 2	$5 \times 5 \times 6$	16	[1,1,1,1]	Same	$14 \times 14 \times 16$
Pool 2	$2 \times 2$	-	[1,2,2,1]	Same	$7 \times 7 \times 16$
FC 1	-	-	-	-	$1024 \times 1$
FC 2	-	-	-	-	$1024 \times 1$
Output	-	-	-	-	$3 \times 1$

configuration for the original OFF-ApexNet architecture is listed in Table 2. The performance result reported range at epoch = [100, 5000]. Apart from testing three streams (where  $p$  and  $q$  images are always remained) for the modified OFF-ApexNet, we also tested single  $p$  direction optical flow as the input. This is to demonstrate that single optical flow component is not sufficient for feature representation and leads to poor recognition performance.

matrix, where  $n$  is the number of kernel. The detailed

## 5. Result and discussion

### 5.1. Variation of Optical Flow Method

The results of varying the optical flow methods using the Bi-WOOF feature extractor and tested on SMIC database is shown in Table 3. It can be seen that TVL1 exhibits the highest accuracy (i.e., 62.20%) and F1-score (i.e., 61.79%). This type of optical flow method has been adopted in several ME recognition systems, such as [65, 18, 67], and promising results are achieved. Horn & Schunck and Lucas Kananade methods have the lowest accuracy. This may due to only a sparse feature sets in the the image are computed. In contrast, TVL1 considers all the pixels in the frame. It is worth noted that, for the Farneback method, although the visualization of the  $p$  and  $q$  images are not showing meaningful ME information (as shown in Figure 7 (a)), the recognition results produced are comparable to that of TVL1.

### 5.2. Adoption of GAN

The results including the training set generated by AC-GAN and SAGAN are tabulated in Table 4. The optical flow images are first reshaped to  $28 \times 28$  before constructing more images. Both the recognition results for AC-GAN and SAGAN are presented, with the Bi-WOOF block size ranged from  $6 \times 6$  to  $25 \times 25$ . The highest accuracy and F1-score obtained are 61.80% and 60.23%, at Bi-WOOF block size =  $15 \times 15$ . For SAGAN, the images are first resized to  $32 \times 32$ . The highest accuracy and F1-score obtained are 62.20% and 0.6109, at Bi-WOOF block size =  $8 \times 8$ . The experimental results are fluctuating throughout the block size. It may imply that the GANs are not stable enough and still have rooms for improvement.

Note that, the the input image size of [42] is  $170 \times 140$ , whereas we reduced 5 times of the original size, and the recognition performance obtained is comparable to that of reported in [42]. To improve the recognition rate, the image size may be increased to better capture and learn the features. Besides, the produced training set (including both the real and fake optical flow images), can be evaluated in the deep learning architecture to observe the impact of the size of data sample.

### 5.3. Modification on OFF-ApexNet

The results of the original OFF-Apexnet (i.e.,  $p$  &  $q$ ) are reproduced and is tabulated in Table 5. In addition, the performance for the single optical flow component (i.e.,  $p$ ) as the input to the modified OFF-ApexNet is reported in the same table for comparison. It can be seen that for  $p$  &  $q$ , the accuracy reached its maximum at epoch = 100 (i.e., 73.01%) and starts to fluctuate afterwards, whereas the F1-score gradually decreases when the epoch iteration increases. On the other hand, for  $p$ , the highest accuracy obtained is 66.21%, when epoch = 2000. In fact, there is not much accuracy difference within the range of epoch = [100, 5000]. It has 7% and 8% lower accuracy

compared to that of  $p$  &  $q$ . Thus, it can be summarized that using a single optical flow component for feature extraction is not sufficient. The best accuracy and F1-score reported in [65] are 74.60% and 0.7104, respectively, at epoch = 3000. However, when we re-implemented the OFF-ApexNet structure with no changes, both the accuracy and F1-score seems to be lower by 1.5%. This amount of deviance is considered acceptable, as the initial parameters (i.e., weights and biases) of the architecture are random, which means that there will be different results for each code execution.

On another note, the recognition results of the proposed three-stream structure which is modified based on the OFF-ApexNet are shown in Table 6. Note that the three features obtained after passing to the two convolutional layers and two pooling layers are multiplied, rather than concatenated. The three input to the architecture are: (1)  $p$  &  $q$  &  $\rho$ ; (2)  $p$  &  $q$  &  $\theta$ ; (3)  $p$  &  $q$  &  $\varepsilon$ ; (4)  $p$  &  $q$  &  $\varepsilon_{ux}$ ; (5)  $p$  &  $q$  &  $\varepsilon_{uy}$ , and; (6)  $p$  &  $q$  &  $\varepsilon_{vx}$ ; It is observed that the results in all the multiplication structure, regardless of the input type, are generally lower than that of with two optical flow components as the input (i.e.,  $p$  &  $q$ ). It is obvious that selecting the magnitude component as the third input would be the least preferable option. For  $p$  &  $q$  &  $\varepsilon$ ,  $p$  &  $q$  &  $\varepsilon_{ux}$  and  $p$  &  $q$  &  $\varepsilon_{uy}$ , the results are comparable, yielding the accuracy of  $\sim 71\%$  and the F1-score of  $\sim 68\%$ .

Furthermore, the results from the principle component analysis (PCA) [86] of certain CNN structures are acquired. Figure 15 and Figure 16 are the examples for the  $p$  &  $q$  &  $\rho$  c, when the CNN architecture is executed at epoch = 0 and epoch = 600, respectively. The three colors refer to the three emotion classes (i.e., surprise, positive and negative). As is shown in these two analysis figure, the classifier fails to distinguish the emotion class at the beginning of the training process (i.e., epoch = 0). After the network has been trained for 600 iterations, it shows an obvious trend that one the features scatters for the same class are clustered in a specific regions. Therefore, it indicates that this PCA analysis is an optimal tool to visualize the training process to have an insight regarding the features learning behavior.

## 6. Conclusion

This paper analyzes several spatio-temporal features and investigates on two generative adversarial networks (GANs) for micro-expression recognition system. First, five optical flow variations are computed (i.e., RLOF, TVL1, Farneback, Lucas Kananade and Horn & Schunck). A thorough comparison among these optical flow methods are reported, where we fix all the experiment configurations to observe the effectiveness of each individual method. Secondly, to deal with the small data size issue and the imbalance of emotion class distribution issues, AC-GAN and SAGAN are employed to generate more artificial micro-expression images. Thirdly, a slight modification on

Table 3: Comparison of recognition accuracy ( $Acc$  (%)) and F1-score ( $F1$ ) for different optical flow methods on SMIC database using Bi-WOOF feature extractor.

block size	Farneback		Horn & Schunck		Lucas Kanade		RLOF		TVL1	
	Acc	F1	Acc	F1	Acc	F1	Acc	F1	Acc	F1
5x5	<b>59.36</b>	<b>.5864</b>	50.64	.4970	<b>53.04</b>	<b>.5284</b>	51.22	.5134	<b>62.20</b>	<b>.6179</b>
6x6	57.53	.5684	50.15	.4983	49.45	.4390	<b>54.27</b>	<b>.5370</b>	57.93	.5756
7x7	57.83	.5726	<b>51.12</b>	<b>0.5082</b>	51.43	0.5103	51.22	.5115	58.54	.5742
8x8	58.54	.5756	50.83	.5067	51.06	.5100	51.83	.5153	57.32	.5672
9x9	57.03	.5644	50.42	.5018	52.13	.5208	53.05	.5302	58.54	.5746
10x10	58.23	.5772	51.03	.4928	52.15	.5212	53.05	.5312	57.93	.5700

Table 4: Comparison of recognition accuracy ( $Acc$  (%)) and F1-score ( $F1$ ) on SMIC database using AC-GAN and SAGAN using Bi-WOOF feature extractor

block size	AC-GAN		SAGAN	
	Acc	F1	Acc	F1
6 × 6	57.01	.4963	59.76	.5854
7 × 7	48.77	.4575	59.76	.5854
8 × 8	50.45	.4972	<b>62.20</b>	<b>.6109</b>
9 × 9	54.42	.4730	61.59	.6034
10 × 10	52.44	.5397	60.37	.5940
11 × 11	58.84	.5194	58.54	.5805
12 × 12	58.90	.4953	60.98	.6029
13 × 13	50.47	.5290	61.59	.6104
14 × 14	53.26	.5442	60.98	.6027
15 × 15	<b>61.80</b>	<b>.6023</b>	59.76	.5872
16 × 16	61.75	.6040	59.15	.5813
17 × 17	58.21	.5860	60.37	.6021
18 × 18	58.82	.5939	59.15	.5885
19 × 19	56.40	.5562	57.93	.5757
20 × 20	56.69	.5477	56.71	.5605
21 × 21	59.35	.5584	57.93	.5717
22 × 22	53.46	.5128	57.93	.5736
23 × 23	53.91	.5303	60.37	.5944
24 × 24	55.54	.5444	59.76	.5903
25 × 25	53.57	.5369	59.76	.5905

a state-of-the-art CNN architecture is made. Comprehensive experiments are conducted and the impact of varying the type of input data are discussed.

For the future works, the GANs generated images with different optical flow methods can be used to enrich the data sample to solve the data imbalance issue. In addition, the modified OFF-ApexNet can be evaluated by receiving the optical flow components computed by other methods,

Table 5: Comparison of recognition accuracy ( $Acc$  (%)) and F1-score ( $F1$ ) on SMIC, CASME II and SAMM databases using the original OFF-ApexNet and  $p$  optical flow component as the input to the modified OFF-ApexNet.

Epoch	$p \ \& \ q$		$p$	
	Acc	F1	Acc	F1
100	<b>73.01</b>	<b>.6964</b>	65.53	.5971
300	71.20	.6805	65.53	.6071
500	69.61	.6631	65.53	.6078
1000	69.84	.6667	65.99	.6103
2000	70.52	.6744	<b>66.21</b>	<b>.6115</b>
3000	70.29	.6712	65.76	.6086
4000	70.75	.6761	65.99	.6113
5000	70.29	.6699	65.53	.6067

such as Farneback, RLOF and Lucas Kanade. Besides, instead of designing the CNN architecture to three parallel stream, it can be extended to more streams to allow automatic high-level feature learning.

## References

- [1] W.-J. Yan, Q. Wu, J. Liang, Y.-H. Chen, and X. Fu, "How fast are the leaked facial expressions: The duration of micro-expressions," *Journal of Nonverbal Behavior*, vol. 37, no. 4, pp. 217–230, 2013.
- [2] A. Vrij and S. Mann, "Police use of nonverbal behavior as indicators of deception," *Applications of nonverbal communication*, ed. *RE Riggio & RS Feldman*, pp. 63–94, 2005.
- [3] J. Endres and A. Laidlaw, "Micro-expression recognition training in medical students: a pilot study," *BMC medical education*, vol. 9, no. 1, p. 47, 2009.
- [4] S. Lodder and Goossens, "Loneliness and the social monitoring system: Emotion recognition and eye gaze in a reallife conversation," *British Journal of Psychology*, vol. 107, pp. 135–153, 2016.
- [5] J. X. Z. Qian, "Grand mediation in chinese rural judicialbased on semi-strangers and endogenous society in the village," *Journal of the Postgraduate of Zhongnan University of Economics and Law*, no. 3, p. 22, 2009.

Table 6: Comparison of recognition accuracy ( $Acc$  (%)) and F1-score ( $F1$ ) on SMIC, CASME II and SAMM databases using the modified OFF-ApexNet.

	$p \ \& \ q \ \& \ \rho$		$p \ \& \ q \ \& \ \theta$		$p \ \& \ q \ \& \ \varepsilon$		$p \ \& \ q \ \& \ \varepsilon_{ux}$		$p \ \& \ q \ \& \ \varepsilon_{uy}$		$p \ \& \ q \ \& \ \varepsilon_{vx}$	
Epoch	Acc	F1	Acc	F1	Acc	F1	Acc	F1	Acc	F1	Acc	F1
100	<b>67.57</b>	.6219	<b>69.16</b>	.6270	69.16	.6450	68.03	.5904	63.49	.5264	63.49	.5260
300	67.12	<b>.6299</b>	68.25	.6446	<b>71.20</b>	<b>.6831</b>	<b>71.88</b>	<b>.6788</b>	<b>71.20</b>	<b>.6764</b>	<b>66.67</b>	<b>.6358</b>
600	66.21	.6228	68.25	.6446	69.61	.6621	69.16	.6548	68.71	.6400	66.44	.6281
1000	66.43	.6287	66.89	<b>.6599</b>	69.61	.6599	69.16	.6548	68.03	.6314	66.21	.6265
2000	66.43	.6287	66.43	.6179	68.70	.6498	68.93	.6413	66.44	.6153	65.08	.6137
3000	65.53	.6216	66.67	.6184	68.25	.6454	68.48	.6450	66.89	.6220	65.08	.6121
4000	65.76	.6256	66.67	.6184	68.25	.6472	68.02	.6402	67.12	.6250	64.62	.6077
5000	65.99	.6289	66.44	.6188	67.80	.6434	68.25	.6434	66.89	.6245	64.62	.6077

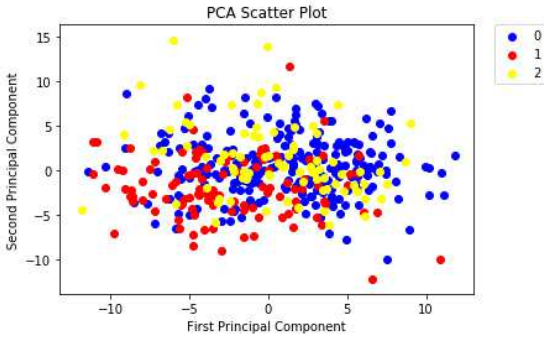


Figure 15: The PCA results for  $p \ \& \ q \ \& \ \rho$  as the input data to the modified OFF-ApexNet, at epoch = 0

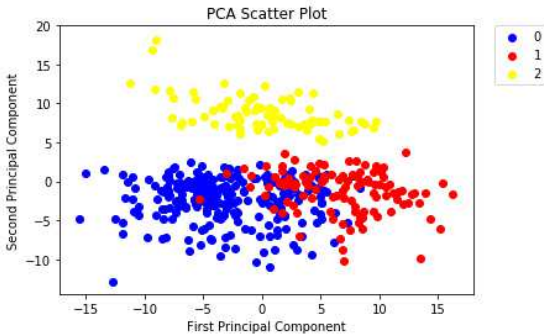


Figure 16: The PCA results for  $p \ \& \ q \ \& \ \rho$  as the input data to the modified OFF-ApexNet, at epoch = 600

[6] P. A. Stewart, B. M. Waller, and J. N. Schubert, "Presidential speechmaking style: Emotional response to micro-expressions of facial affect," *Motivation and Emotion*, vol. 33, no. 2, p. 125, 2009.

[7] M. Holmes, "National security behavioral detection: a typography of strategies, costs, and benefits," *Journal of Transportation Security*, vol. 4, no. 4, p. 361, 2011.

[8] P. Ekman and W. V. Friesen, "Nonverbal leakage and clues to deception," *Psychiatry*, vol. 32, no. 1, pp. 88–106, 1969.

[9] P. Ekman and W. V. Friesen, "Facial action coding system consulting psychologists press," *Palo Alto, CA*, 1978.

[10] X. Li, X. Hong, A. Moilanen, X. Huang, T. Pfister, G. Zhao, and M. Pietikäinen, "Towards reading hidden emotions: A compar-

ative study of spontaneous micro-expression spotting and recognition methods," *IEEE Transactions on Affective Computing*, vol. 9, no. 4, pp. 563–577, 2018.

[11] M. Shreve, S. Godavarthy, D. Goldgof, and S. Sarkar, "Macro- and micro-expression spotting in long videos using spatio-temporal strain," in *Face and Gesture 2011*, pp. 51–56, IEEE, 2011.

[12] T. Pfister, X. Li, G. Zhao, and M. Pietikäinen, "Recognising spontaneous facial micro-expressions," in *2011 international conference on computer vision*, pp. 1449–1456, IEEE, 2011.

[13] X. Li, T. Pfister, X. Huang, G. Zhao, and M. Pietikäinen, "A spontaneous micro-expression database: Inducement, collection and baseline," in *2013 10th IEEE International Conference and Workshops on Automatic Face and Gesture Recognition (FG)*, pp. 1–6, IEEE, 2013.

[14] W.-J. Yan, Q. Wu, Y.-J. Liu, S.-J. Wang, and X. Fu, "Casme database: a dataset of spontaneous micro-expressions collected from neutralized faces," in *2013 10th IEEE international conference and workshops on automatic face and gesture recognition (FG)*, pp. 1–7, IEEE, 2013.

[15] W.-J. Yan, X. Li, S.-J. Wang, G. Zhao, Y.-J. Liu, Y.-H. Chen, and X. Fu, "Casme ii: An improved spontaneous micro-expression database and the baseline evaluation," *PloS one*, vol. 9, no. 1, p. e86041, 2014.

[16] F. Qu, S.-J. Wang, W.-J. Yan, H. Li, S. Wu, and X. Fu, "Cas ( $me$ )<sup>2</sup>: A database for spontaneous macro-expression and micro-expression spotting and recognition," *IEEE Transactions on Affective Computing*, vol. 9, no. 4, pp. 424–436, 2018.

[17] A. K. Davison, C. Lansley, N. Costen, K. Tan, and M. H. Yap, "Samm: A spontaneous micro-facial movement dataset," *IEEE Transactions on Affective Computing*, vol. 9, no. 1, pp. 116–129, 2018.

[18] S. T. Liong, *Micro-expression recognition analysis using facial strain/Liong Sze Teng*. PhD thesis, University of Malaya, 2017.

[19] T. F. Cootes, C. J. Taylor, D. H. Cooper, and J. Graham, "Active shape models-their training and application," *Computer vision and image understanding*, vol. 61, no. 1, pp. 38–59, 1995.

[20] G. J. Edwards, T. F. Cootes, and C. J. Taylor, "Face recognition using active appearance models," in *European conference on computer vision*, pp. 581–595, Springer, 1998.

[21] A. Asthana, S. Zafeiriou, S. Cheng, and M. Pantic, "Robust discriminative response map fitting with constrained local models," in *Proceedings of the IEEE conference on computer vision and pattern recognition*, pp. 3444–3451, 2013.

[22] Z. Xia, X. Feng, J. Peng, X. Peng, and G. Zhao, "Spontaneous micro-expression spotting via geometric deformation modeling," *Computer Vision and Image Understanding*, vol. 147, pp. 87–94, 2016.

[23] P. Dollár, P. Welinder, and P. Perona, "Cascaded pose regres-

- sion,” in *2010 IEEE Computer Society Conference on Computer Vision and Pattern Recognition*, pp. 1078–1085, IEEE, 2010.
- [24] H. Drucker, C. J. Burges, L. Kaufman, A. J. Smola, and V. Vapnik, “Support vector regression machines,” in *Advances in neural information processing systems*, pp. 155–161, 1997.
- [25] Q. Zhu, M.-C. Yeh, K.-T. Cheng, and S. Avidan, “Fast human detection using a cascade of histograms of oriented gradients,” in *2006 IEEE Computer Society Conference on Computer Vision and Pattern Recognition (CVPR’06)*, vol. 2, pp. 1491–1498, IEEE, 2006.
- [26] “Face++ research toolkit.” <https://www.faceplusplus.com>, 2013.
- [27] B. Amos, B. Ludwiczuk, and M. Satyanarayanan, “Openface: A general-purpose face recognition library with mobile applications,” tech. rep., CMU-CS-16-118, CMU School of Computer Science, 2016.
- [28] Y. Sun, X. Wang, and X. Tang, “Deep convolutional network cascade for facial point detection,” in *Proceedings of the IEEE conference on computer vision and pattern recognition*, pp. 3476–3483, 2013.
- [29] Z. Huang, E. Zhou, and Z. Cao, “Coarse-to-fine face alignment with multi-scale local patch regression,” *arXiv preprint arXiv:1511.04901*, 2015.
- [30] K. Zhang, Z. Zhang, Z. Li, and Y. Qiao, “Joint face detection and alignment using multitask cascaded convolutional networks,” *IEEE Signal Processing Letters*, vol. 23, no. 10, pp. 1499–1503, 2016.
- [31] M. Kowalski, J. Naruniec, and T. Trzcinski, “Deep alignment network: A convolutional neural network for robust face alignment,” in *Proceedings of the IEEE Conference on Computer Vision and Pattern Recognition Workshops*, pp. 88–97, 2017.
- [32] A. Davison, W. Merghani, C. Lansley, C.-C. Ng, and M. H. Yap, “Objective micro-facial movement detection using face-based regions and baseline evaluation,” in *2018 13th IEEE International Conference on Automatic Face & Gesture Recognition (FG 2018)*, pp. 642–649, IEEE, 2018.
- [33] A. Goshtasby, “Image registration by local approximation methods,” *Image and Vision Computing*, vol. 6, no. 4, pp. 255–261, 1988.
- [34] S.-T. Liong, J. See, K. Wong, and R. C.-W. Phan, “Automatic micro-expression recognition from long video using a single spotted apex,” in *Asian Conference on Computer Vision*, pp. 345–360, Springer, 2016.
- [35] A. Moilanen, G. Zhao, and M. Pietikäinen, “Spotting rapid facial movements from videos using appearance-based feature difference analysis,” in *2014 22nd International Conference on Pattern Recognition*, pp. 1722–1727, IEEE, 2014.
- [36] A. K. Davison, M. H. Yap, and C. Lansley, “Micro-facial movement detection using individualised baselines and histogram-based descriptors,” in *2015 IEEE International Conference on Systems, Man, and Cybernetics*, pp. 1864–1869, IEEE, 2015.
- [37] S.-J. Wang, S. Wu, and X. Fu, “A main directional maximal difference analysis for spotting micro-expressions,” in *Asian Conference on Computer Vision*, pp. 449–461, Springer, 2016.
- [38] S.-T. Liong, J. See, R. C.-W. Phan, A. C. Le Ngo, Y.-H. Oh, and K. Wong, “Subtle expression recognition using optical strain weighted features,” in *Asian Conference on Computer Vision*, pp. 644–657, Springer, 2014.
- [39] S. Polikovskiy, Y. Kameda, and Y. Ohta, “Facial micro-expressions recognition using high speed camera and 3d-gradient descriptor,” 2009.
- [40] S. Polikovskiy, Y. Kameda, and Y. Ohta, “Facial micro-expression detection in hi-speed video based on facial action coding system (facs),” *IEICE transactions on information and systems*, vol. 96, no. 1, pp. 81–92, 2013.
- [41] S.-T. Liong, J. See, K. Wong, A. C. Le Ngo, Y.-H. Oh, and R. Phan, “Automatic apex frame spotting in micro-expression database,” in *2015 3rd IAPR Asian Conference on Pattern Recognition (ACPR)*, pp. 665–669, IEEE, 2015.
- [42] S.-T. Liong, J. See, K. Wong, and R. C.-W. Phan, “Less is more: Micro-expression recognition from video using apex frame,” *Signal Processing: Image Communication*, vol. 62, pp. 82–92, 2018.
- [43] S.-T. Liong, J. See, R. C.-W. Phan, K. Wong, and S.-W. Tan, “Hybrid facial regions extraction for micro-expression recognition system,” *Journal of Signal Processing Systems*, vol. 90, no. 4, pp. 601–617, 2018.
- [44] J. Li, C. Soladie, and R. Seguier, “Ltp-ml: micro-expression detection by recognition of local temporal pattern of facial movements,” in *2018 13th IEEE International Conference on Automatic Face & Gesture Recognition (FG 2018)*, pp. 634–641, IEEE, 2018.
- [45] M. Shreve, J. Brizzi, S. Fefilyayev, T. Luguev, D. Goldgof, and S. Sarkar, “Automatic expression spotting in videos,” *Image and Vision Computing*, vol. 32, no. 8, pp. 476–486, 2014.
- [46] Z. Zhou, G. Zhao, and M. Pietikäinen, “Towards a practical lipreading system,” in *CVPR 2011*, pp. 137–144, IEEE, 2011.
- [47] S.-J. Wang, W.-J. Yan, G. Zhao, X. Fu, and C.-G. Zhou, “Micro-expression recognition using robust principal component analysis and local spatiotemporal directional features,” in *Workshop at the European conference on computer vision*, pp. 325–338, Springer, 2014.
- [48] A. C. Le Ngo, J. See, and R. C.-W. Phan, “Sparsity in dynamics of spontaneous subtle emotions: analysis and application,” *IEEE Transactions on Affective Computing*, vol. 8, no. 3, pp. 396–411, 2017.
- [49] H.-Y. Wu, M. Rubinstein, E. Shih, J. Guttag, F. Durand, and W. Freeman, “Eulerian video magnification for revealing subtle changes in the world,” 2012.
- [50] A. C. Le Ngo, A. Johnston, R. C.-W. Phan, and J. See, “Micro-expression motion magnification: Global lagrangian vs. local eulerian approaches,” in *2018 13th IEEE International Conference on Automatic Face & Gesture Recognition (FG 2018)*, pp. 650–656, IEEE, 2018.
- [51] T. Ojala, M. Pietikäinen, and D. Harwood, “A comparative study of texture measures with classification based on featured distributions,” *Pattern recognition*, vol. 29, no. 1, pp. 51–59, 1996.
- [52] G. Zhao and M. Pietikainen, “Dynamic texture recognition using local binary patterns with an application to facial expressions,” *IEEE Transactions on Pattern Analysis & Machine Intelligence*, no. 6, pp. 915–928, 2007.
- [53] C. House and R. Meyer, “Preprocessing and descriptor features for facial micro-expression recognition,” 2015.
- [54] Y. Wang, J. See, R. C.-W. Phan, and Y.-H. Oh, “Lbp with six intersection points: Reducing redundant information in lbp-top for micro-expression recognition,” in *Asian conference on computer vision*, pp. 525–537, Springer, 2014.
- [55] Y. Wang, J. See, R. C.-W. Phan, and Y.-H. Oh, “Efficient spatio-temporal local binary patterns for spontaneous facial micro-expression recognition,” *PloS one*, vol. 10, no. 5, pp. 1–20, 2015.
- [56] H. Xiaohua, S.-J. Wang, X. Liu, G. Zhao, X. Feng, and M. Pietikainen, “Discriminative spatiotemporal local binary pattern with revisited integral projection for spontaneous facial micro-expression recognition,” *IEEE Transactions on Affective Computing*, 2017.
- [57] X. Huang, G. Zhao, X. Hong, W. Zheng, and M. Pietikäinen, “Spontaneous facial micro-expression analysis using spatiotemporal completed local quantized patterns,” *Neurocomputing*, vol. 175, pp. 564–578, 2016.
- [58] S.-J. Wang, W.-J. Yan, X. Li, G. Zhao, and X. Fu, “Micro-expression recognition using dynamic textures on tensor independent color space,” in *2014 22nd International Conference on Pattern Recognition*, pp. 4678–4683, IEEE, 2014.
- [59] S. Happy and A. Routray, “Fuzzy histogram of optical flow orientations for micro-expression recognition,” *IEEE Transactions on Affective Computing*, 2017.
- [60] F. Xu, J. Zhang, and J. Z. Wang, “Microexpression identification and categorization using a facial dynamics map,” *IEEE Transactions on Affective Computing*, vol. 8, no. 2, pp. 254–267,

- 2017.
- [61] Y.-J. Liu, J.-K. Zhang, W.-J. Yan, S.-J. Wang, G. Zhao, and X. Fu, "A main directional mean optical flow feature for spontaneous micro-expression recognition," *IEEE Transactions on Affective Computing*, vol. 7, no. 4, pp. 299–310, 2016.
- [62] N. Dalal and B. Triggs, "Histograms of oriented gradients for human detection," in *international Conference on computer vision & Pattern Recognition (CVPR'05)*, vol. 1, pp. 886–893, IEEE Computer Society, 2005.
- [63] M. Peng, C. Wang, T. Chen, G. Liu, and X. Fu, "Dual temporal scale convolutional neural network for micro-expression recognition," *Frontiers in psychology*, vol. 8, p. 1745, 2017.
- [64] D. H. Kim, W. Baddar, J. Jang, and Y. M. Ro, "Multi-objective based spatio-temporal feature representation learning robust to expression intensity variations for facial expression recognition," *IEEE Transactions on Affective Computing*, no. 1, pp. 1–1, 2017.
- [65] S.-T. Liong, Y. Gan, W.-C. Yau, Y.-C. Huang, and T. L. Ken, "Off-apexnet on micro-expression recognition system," *arXiv preprint arXiv:1805.08699*, 2018.
- [66] S.-T. Liong, Y. Gan, J. See, and H.-Q. Khor, "A shallow triple stream three-dimensional cnn (ststnet) for micro-expression recognition system," *arXiv preprint arXiv:1902.03634*, 2019.
- [67] Y. Gan and S.-T. Liong, "Bi-directional vectors from apex in cnn for micro-expression recognition," in *2018 IEEE 3rd International Conference on Image, Vision and Computing (ICIVC)*, pp. 168–172, IEEE, 2018.
- [68] Z. Zhang, T. Chen, H. Meng, G. Liu, and X. Fu, "Smeconvnet: A convolutional neural network for spotting spontaneous facial micro-expression from long videos," *IEEE Access*, vol. 6, pp. 71143–71151, 2018.
- [69] D. Patel, X. Hong, and G. Zhao, "Selective deep features for micro-expression recognition," in *2016 23rd International Conference on Pattern Recognition (ICPR)*, pp. 2258–2263, IEEE, 2016.
- [70] M. A. Takalkar and M. Xu, "Image based facial micro-expression recognition using deep learning on small datasets," in *2017 International Conference on Digital Image Computing: Techniques and Applications (DICTA)*, pp. 1–7, IEEE, 2017.
- [71] S. R. Gunn *et al.*, "Support vector machines for classification and regression," *ISIS technical report*, vol. 14, no. 1, pp. 5–16, 1998.
- [72] A. Liaw, M. Wiener, *et al.*, "Classification and regression by randomforest," *R news*, vol. 2, no. 3, pp. 18–22, 2002.
- [73] J. Yang, L. Zhang, Y. Xu, and J.-y. Yang, "Beyond sparsity: The role of l1-optimizer in pattern classification," *Pattern Recognition*, vol. 45, no. 3, pp. 1104–1118, 2012.
- [74] H. Zheng, X. Geng, and Z. Yang, "A relaxed k-svd algorithm for spontaneous micro-expression recognition," in *Pacific Rim International Conference on Artificial Intelligence*, pp. 692–699, Springer, 2016.
- [75] Y. Gan, S.-T. Liong, W.-C. Yau, Y.-C. Huang, and L.-K. Tan, "Off-apexnet on micro-expression recognition system," *Signal Processing: Image Communication*, vol. 74, pp. 129–139, 2019.
- [76] T. Senst, V. Eiselein, and T. Sikora, "Robust local optical flow for feature tracking," *IEEE Transactions on Circuits and Systems for Video Technology*, vol. 22, no. 9, pp. 1377–1387, 2012.
- [77] B. K. Horn and B. G. Schunck, "Determining optical flow," *Artificial intelligence*, vol. 17, no. 1-3, pp. 185–203, 1981.
- [78] A. Wedel, T. Pock, J. Braun, U. Franke, and D. Cremers, "Duality tv-l1 flow with fundamental matrix prior," in *2008 23rd International Conference Image and Vision Computing New Zealand*, pp. 1–6, IEEE, 2008.
- [79] G. Farneback, "Two-frame motion estimation based on polynomial expansion," in *Scandinavian conference on Image analysis*, pp. 363–370, Springer, 2003.
- [80] T.-W. Hui, X. Tang, and C. Change Loy, "Liteflownet: A lightweight convolutional neural network for optical flow estimation," in *Proceedings of the IEEE Conference on Computer Vision and Pattern Recognition*, pp. 8981–8989, 2018.
- [81] D. Sun, X. Yang, M.-Y. Liu, and J. Kautz, "Pwc-net: Cnns for optical flow using pyramid, warping, and cost volume," in *Proceedings of the IEEE Conference on Computer Vision and Pattern Recognition*, pp. 8934–8943, 2018.
- [82] A. Dosovitskiy, P. Fischer, E. Ilg, P. Hausser, C. Hazirbas, V. Golkov, P. Van Der Smagt, D. Cremers, and T. Brox, "Flownet: Learning optical flow with convolutional networks," in *Proceedings of the IEEE international conference on computer vision*, pp. 2758–2766, 2015.
- [83] J. L. Barron, D. J. Fleet, S. S. Beauchemin, and T. Burkitt, "Performance of optical flow techniques," in *Proceedings 1992 IEEE Computer Society Conference on Computer Vision and Pattern Recognition*, pp. 236–242, IEEE, 1992.
- [84] A. Odena, C. Olah, and J. Shlens, "Conditional image synthesis with auxiliary classifier gans," in *Proceedings of the 34th International Conference on Machine Learning-Volume 70*, pp. 2642–2651, JMLR. org, 2017.
- [85] H. Zhang, I. Goodfellow, D. Metaxas, and A. Odena, "Self-attention generative adversarial networks," *arXiv preprint arXiv:1805.08318*, 2018.
- [86] S. Wold, K. Esbensen, and P. Geladi, "Principal component analysis," *Chemometrics and intelligent laboratory systems*, vol. 2, no. 1-3, pp. 37–52, 1987.